AD-A080 533 OKLAHOMA UNIV NORMAN SCHOOL OF AEROSPACE MECHANICAL --ETC F/G 11/4
A COMPARISON OF CLOSED-FORM AND FINITE-ELEMENT SOLUTIONS OF THI--ETC(U)
DEC 79 J N REDDY N00014-78-C-0647
UNCLASSIFIED OU-AMNE-79-19 NL

| OF |
AD
A080533

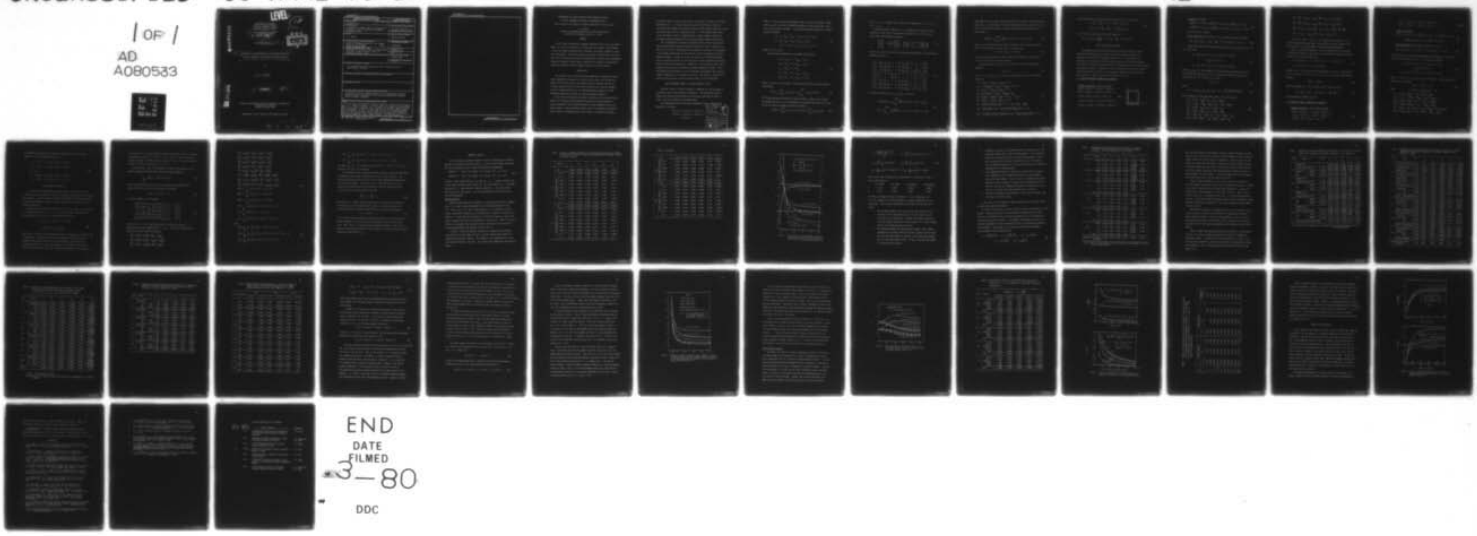

END
DATE
FILMED
3-80
DDC

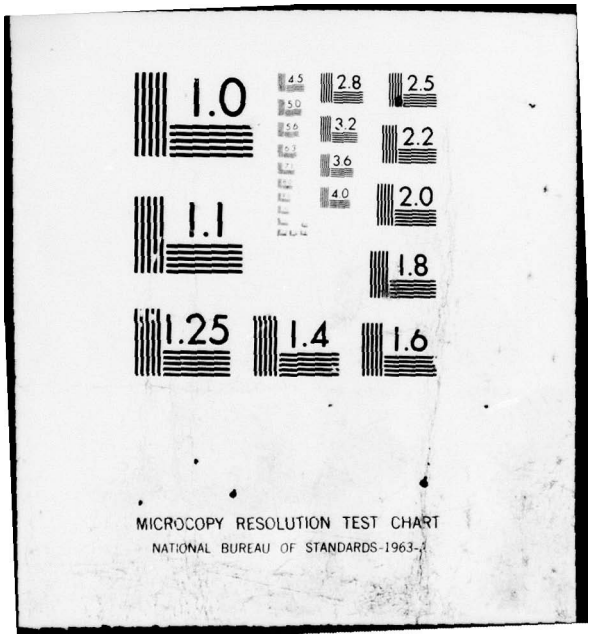
1.0
1.1
1.25
1.4
1.6
1.8
2.0
2.2
2.5
2.8
3.2
3.6
4.0
4.5
5.0
5.6
6.3
MICROCOPY RESOLUTION TEST CHART
NATIONAL BUREAU OF STANDARDS-1963-A

LEVEL II

12

Department of the Navy
OFFICE OF NAVAL RESEARCH
Structural Mechanics Program
Arlington, Virginia 22217

(15) Contract N00014-78-C-0647
Project NR 064-609
(9) Technical Report No. 8

(14) Report OU-AMNE-79-19, TR-8

(6) A COMPARISON OF CLOSED-FORM AND FINITE-ELEMENT SOLUTIONS OF THICK, LAMINATED, ANISOTROPIC RECTANGULAR PLATES.

by

(10) J. N. Reddy

(11) December 1979

(12) 42

School of Aerospace, Mechanical and Nuclear Engineering
University of Oklahoma
Norman, Oklahoma 73019

400 498

UNCLASSIFIED

SECURITY CLASSIFICATION OF THIS PAGE (When Data Entered)

REPORT DOCUMENTATION PAGE		READ INSTRUCTIONS BEFORE COMPLETING FORM
1. REPORT NUMBER OU-AMNE-79-19	2. GOVT ACCESSION NO.	3. RECIPIENT'S CATALOG NUMBER
4. TITLE (and Subtitle) A COMPARISON OF CLOSED-FORM AND FINITE-ELEMENT SOLUTIONS OF THICK, LAMINATED, ANISOTROPIC RECTANGULAR PLATES		5. TYPE OF REPORT & PERIOD COVERED Technical Report No. 8 6. PERFORMING ORG. REPORT NUMBER
7. AUTHOR(s) J. N. Reddy		8. CONTRACT OR GRANT NUMBER(s) N00014-78-C-0647
9. PERFORMING ORGANIZATION NAME AND ADDRESS School of Aerospace, Mechanical and Nuclear Engrg. University of Oklahoma Norman, Oklahoma 73019		10. PROGRAM ELEMENT, PROJECT, TASK AREA & WORK UNIT NUMBERS NR 064-609
11. CONTROLLING OFFICE NAME AND ADDRESS Department of the Navy, Office of Naval Research Structural Mechanics Program (Code 474) Arlington, Virginia 22217		12. REPORT DATE December 1979 13. NUMBER OF PAGES 40
14. MONITORING AGENCY NAME & ADDRESS(if different from Controlling Office)		15. SECURITY CLASS. (of this report) Unclassified 15a. DECLASSIFICATION/ DOWNGRADING SCHEDULE

16. DISTRIBUTION STATEMENT (of this Report)

This document has been approved for public release and sale; distribution unlimited.

17. DISTRIBUTION STATEMENT (of the abstract entered in Block 20, if different from Report)

18. SUPPLEMENTARY NOTES

19. KEY WORDS (Continue on reverse side if necessary and identify by block number)

Closed-form solutions, composite materials, finite-element solutions, laminated plates, rectangular plates, reduced integration, stresses, thermal bending, vibrations.

20. ABSTRACT (Continue on reverse side if necessary and identify by block number)

In this study the effects of reduced integration, mesh size, and element type (i.e. linear or quadratic) on the accuracy of a penalty finite element based on the theory governing thick, laminated, anisotropic composite plates, are investigated. In order to assess the accuracy of the present element, exact closed-form solutions are developed for cross-ply and antisymmetric angle-ply rectangular plates simply supported and subjected to sinusoidally distributed mechanical and/or thermal loadings, and free vibration.

DD FORM 1 JAN 73 1473 EDITION OF 1 NOV 65 IS OBSOLETE
S/N 0102-014-6601 |

UNCLASSIFIED

SECURITY CLASSIFICATION OF THIS PAGE (When Data Entered)

A COMPARISON OF CLOSED-FORM AND FINITE-ELEMENT SOLUTIONS OF THICK, LAMINATED, ANISOTROPIC RECTANGULAR PLATES

(with a study of the effect of reduced integration on the accuracy)

J. N. Reddy
School of Aerospace, Mechanical and Nuclear Engineering
University of Oklahoma, Norman, OK 73019

SUMMARY

In this study the effects of reduced integration, mesh size, and element type (i.e. linear or quadratic) on the accuracy of a penalty finite element based on the theory governing thick, laminated, anisotropic composite plates, are investigated. In order to assess the accuracy of the present finite element, exact closed-form solutions are developed for cross-ply and antisymmetric angle-ply rectangular plates simply supported and subjected to sinusoidally distributed mechanical and/or thermal loadings, and free vibration.

INTRODUCTION

The increased use of fiber-reinforced composites in aerospace and mechanical engineering structures is primarily due to their high stiffness-to-weight ratio and due to their anisotropic material property that can be tailored through variation of the fiber orientation and stacking sequence. With the increased application, the thermo-mechanical behavior of fiber-reinforced composite structures is receiving greater attention.

Due to the low transverse shear moduli relative to the in-plane Young's moduli, the transverse shear deformation effects are more pronounced in plates laminated of fiber-reinforced materials when compared to thick isotropic plates. A shear deformable theory that is an extension of Reissner-Mindlin theory for homogeneous isotropic plates to arbitrarily laminated

anisotropic plates is due to Yang, Norris, and Stavsky [1] (see also, Whitney and Pagano [2]). In a recent study the author [3,4] derived, using the penalty-function method, the Yang-Norris-Stavsky (YNS) theory from the classical thin-plate theory (CPT) of laminated plates. A finite-element model based on the YNS theory results in computationally simpler elements compared to previously reported elements [5-8], and yet possesses competitive accuracy.

This investigation is primarily concerned with a critical study of the penalty plate-bending element developed by the author [3,4]. Specifically, the study involves an investigation of the numerical accuracy and convergence of the element when applied to the analysis of thick, laminated anisotropic composite plates. In order to assess the accuracy of the present element, exact closed-form solutions are also derived for freely supported rectangular plates of cross-ply construction. Comparison is also made with other finite-element solutions, and 3-D elasticity solutions wherever available. Since the penalty-function method is used in developing the element, the so-called reduced integration [9,10] comes into picture. The effect of reduced integration on the accuracy of thin and thick plates is also investigated.

SHEAR DEFORMABLE THEORY OF LAYERED COMPOSITE PLATES

Consider a plate of uniform thickness t composed of a finite number of anisotropic layers with arbitrary orientations. The coordinate system is chosen such that the middle plane, R, of the plate coincides with the x-y plane, with z-axis normal to the middle plane.

The displacement field in the shear deformable theory of Whitney and Pagano [2] is given by

$$u(x,y,z,\tau) = u_0(x,y,\tau) + z\psi_x(x,y,\tau)$$
$$v(x,y,z,\tau) = v_0(x,y,\tau) + z\psi_y(x,y,\tau)$$
$$w = w(x,y,\tau)$$

where u, v, and w are the displacements along x, y and z directions, respectively, u_o and v_o are the in-plane displacements of the middle plane, and ψ_x and ψ_y are the shear rotations. The strain-displacement equations of linear elasticity become,

$$\varepsilon_1 \equiv \varepsilon_x = u_{o,x} + z\psi_{x,x} \ , \ \varepsilon_2 \equiv \varepsilon_y = v_{o,y} + z\psi_{y,y},$$

$$\varepsilon_6 \equiv \gamma_{xy} = u_{o,y} + v_{o,x} + z(\psi_{x,y} + \psi_{y,x}) \ , \tag{2}$$

$$\gamma_{xz} = \psi_x + w_{,x} \ , \ \gamma_{yz} = \psi_y + w_{,y} \ , \ \varepsilon_z = 0$$

where $w_{,x} \equiv \partial w/\partial x$, etc.

The equilibrium equations of the theory are given by,

$$\begin{aligned}
N_{1,x} + N_{6,y} &= P_1 + Ru_{o,\tau\tau} + S\psi_{x,\tau\tau} \\
N_{6,x} + N_{2,y} &= P_2 + Rv_{o,\tau\tau} + S\psi_{y,\tau\tau} \\
Q_{1,x} + Q_{2,y} &= P_3 + Rw_{,\tau\tau} \\
M_{1,x} + M_{6,y} - Q_1 &= I\psi_{x,\tau\tau} + S\, u_{o,\tau\tau} \\
M_{6,x} + M_{2,y} - Q_2 &= I\psi_{y,\tau\tau} + S\, v_{o,\tau\tau}
\end{aligned} \tag{3}$$

where R, S, and I are the normal, coupled normal-rotary, and rotary inertia coefficients,

$$(R,S,I) = \int_{-t/2}^{t/2} (1,z,z^2)\, \rho dz = \sum_m \int_{z_m}^{z_{m+1}} (1,z,z^2)\, \rho^{(m)}\, dz \tag{4}$$

$\rho^{(m)}$ being the material density of the m-th layer, P_1 and P_2 are in-plane distributed forces, P_3 is the transversely distributed force, and N_i, Q_i, and M_i are the stress and moment resultants defined by

$$(N_i,M_i) = \int_{-t/2}^{t/2} (1,z)\, \sigma_i\, dz \ , \ (Q_1,Q_2) = \int_{-t/2}^{t/2} (\sigma_{xy},\sigma_{yz})\, dz \tag{5}$$

Here σ_i (i = 1,2,6) denote the in-plane stress components ($\sigma_1 = \sigma_x$, $\sigma_2 = \sigma_y$, and $\sigma_6 = \sigma_{xy}$).

Assuming monoclinic behavior (i.e., existence of one plane of elastic symmetry) for each layer, the constitutive equations for the m-th layer (in the plate coordinates) are given by

$$\begin{Bmatrix} \sigma_1 \\ \sigma_2 \\ \sigma_6 \end{Bmatrix} = [Q_{ij}^{(m)}] \begin{Bmatrix} \varepsilon_1 \\ \varepsilon_2 \\ \varepsilon_6 \end{Bmatrix}, \quad \begin{Bmatrix} \tau_{xz} \\ \tau_{yz} \end{Bmatrix} = \begin{bmatrix} Q_{44} & Q_{45} \\ Q_{45} & Q_{55} \end{bmatrix} \begin{Bmatrix} \gamma_{xz} \\ \gamma_{yz} \end{Bmatrix} \tag{6}$$

so that (in view of (5) and (6)) the constitutive equations for an arbitrarily laminated plate are

$$\begin{Bmatrix} N_1 \\ N_2 \\ N_6 \\ Q_1 \\ Q_2 \\ M_1 \\ M_2 \\ M_6 \end{Bmatrix} = \begin{bmatrix} A_{11} & A_{12} & A_{16} & 0 & 0 & B_{11} & B_{12} & B_{16} \\ A_{12} & A_{22} & A_{26} & 0 & 0 & B_{12} & B_{22} & B_{26} \\ A_{16} & A_{26} & A_{66} & 0 & 0 & B_{16} & B_{26} & B_{66} \\ 0 & 0 & 0 & A_{44} & A_{45} & 0 & 0 & 0 \\ 0 & 0 & 0 & A_{45} & A_{55} & 0 & 0 & 0 \\ B_{11} & B_{12} & B_{16} & 0 & 0 & D_{11} & D_{12} & D_{16} \\ B_{12} & B_{22} & B_{26} & 0 & 0 & D_{12} & D_{22} & D_{26} \\ B_{16} & B_{26} & B_{66} & 0 & 0 & D_{16} & D_{26} & D_{66} \end{bmatrix} \begin{Bmatrix} u_{o,x} \\ v_{o,y} \\ u_{o,y}+v_{o,x} \\ w_{,x}+\psi_x \\ w_{,y}+\psi_y \\ \psi_{x,x} \\ \psi_{y,y} \\ \psi_{x,y}+\psi_{y,x} \end{Bmatrix} - \begin{Bmatrix} N_1^T \\ N_2^T \\ N_6^T \\ 0 \\ 0 \\ M_1^T \\ M_2^T \\ M_6^T \end{Bmatrix} \tag{7}$$

The plate stiffnesses A_{ij}, B_{ij}, and D_{ij} are given by

$$\begin{aligned} (A_{ij},B_{ij},D_{ij}) &= \sum_m \int_{z_m}^{z_{m+1}} Q_{ij}^{(m)}(1,z,z^2)\, dz \,, \quad (i,j = 1,2,6) \\ A_{ij} &= \sum_m \int_{z_m}^{z_{m+1}} k_\alpha k_\beta Q_{ij}^{(m)}\, dz \,, \quad (\alpha = 6-i,\ \beta = 6-j;\ i,j = 4,5) \end{aligned} \tag{8}$$

where $Q_{ij}^{(m)}$ are the stiffness coefficients of the m-th layer in the plate coordinates, and z_m is the distance from the mid-plane to the lower surface of the m-th layer. The stress and moment resultants, N_i^T and M_i^T, due to thermal loading are defined by

$$(N_i^T, M_i^T) = \sum_m \int_{z_m}^{z_{m+1}} \sum_j Q_{ij}^{(m)} \alpha_j (T_o, zT_1)\, dz \ , \ (i,j = 1,2,6) \tag{9}$$

where α_i are the thermal coefficients of expansion in the plate coordinates, and T is the temperature change from a reference state,

$$T(x,y,z) = T_o(x,y) + zT_1(x,y) \tag{10}$$

Note that the temperature variation through the thickness is assumed to be linear, consistent with the plate theory.

Substituting Eq. (7) into Eq. (3), we obtain the following operator equation,

$$[L]\{\delta\} = \{f\} \tag{11}$$

where $\{\delta\} = \{u_o, v_o, w, \psi_x, \psi_y\}^T$, [L] is the (symmetric) matrix of differential operators,

$$\begin{aligned}
L_{11} &= A_{11}d_{11} + 2A_{16}d_{12} + A_{66}d_{22} + R\,d_{\tau\tau} \\
L_{12} &= (A_{12}+A_{66})d_{12} + A_{16}d_{11} + A_{26}d_{22} \ , \ L_{13} = 0 \ , \\
L_{14} &= B_{11}d_{11} + 2B_{16}d_{12} + B_{66}d_{22} + S\,d_{\tau\tau} \\
L_{15} &= (B_{12}+B_{66})d_{12} + B_{16}d_{11} + B_{26}d_{22} = L_{24} \ , \\
L_{22} &= 2A_{26}d_{12} + A_{22}d_{22} + A_{66}d_{11} + R\,d_{\tau\tau} \ , \ L_{23} = 0 \\
L_{25} &= 2B_{26}d_{12} + B_{22}d_{22} + B_{66}d_{11} + S\,d_{\tau\tau} \\
L_{33} &= -A_{44}d_{11} - 2A_{45}d_{12} - A_{55}d_{22} + R\,d_{\tau\tau} \ , \ L_{34} = A_{44}d_1 - A_{45}d_2 \\
L_{35} &= -A_{45}d_1 - A_{55}d_2 \ , \ L_{44} = D_{11}d_{11} + 2D_{16}d_{12} + D_{66}d_{22} - A_{44} + I\,d_{\tau\tau} \\
L_{45} &= (D_{12}+D_{66})d_{12} + D_{16}d_{11} + D_{26}d_{22} - A_{45} \ , \ L_{55} = 2D_{26}d_{12} + D_{22}d_{22} + D_{66}d_{11} + I\,d_{\tau\tau}
\end{aligned} \tag{12}$$

and the components of the generalized force vector, $\{f\}$, are given by

$$f_1 = N^T_{1,x} + N^T_{6,y} + P_1 \ , \ f_2 = N^T_{6,x} + N^T_{2,y} + P_2$$
$$f_3 = P_3 \ , \ f_4 = M^T_{1,x} + M^T_{6,y} \ , \ f_5 = M^T_{6,x} + M_{2,y} \tag{13}$$

In Eq. (12), d_{ij} denote the differential operators

$$d_\tau = \partial/\partial\tau, \ d_{ij} = \frac{\partial^2}{\partial x_i \partial x_j} \ , \ d_i = d_{io} = \frac{\partial}{\partial x_i} \ , \ (i,j = 0,1,2)$$

EXACT CLOSED-FORM SOLUTIONS

The boundary-value problem associated with the equilibrium of layered anisotropic composite plates involves solving the operator equation (11) subjected to a given set of boundary conditions. It is not possible to construct exact solutions to Eq. (11) when the plate is of arbitrary geometry, constructed of arbitrarily-oriented layers, and subjected to an arbitrary loading or boundary conditions. However, an exact closed-form solution to Eq. (11) can be constructed when the plate is of rectangular geometry with the following edge conditions, loading, and plate construction (cf. [2]).

A. Cross-Ply Plates in Bending and Vibration

Boundary conditions (freely supported)

$$u_o(x,0) = u_o(x,b) = 0, \ N_2(x,0) = N_2(x,b) = 0$$
$$v_o(0,y) = v_o(a,y) = 0, \ N_1(0,y) = N_1(a,y) = 0$$
$$w(x,0) = w(x,b) = w(0,y) = w(a,y) = 0 \tag{14}$$
$$\psi_x(x,0) = \psi_x(x,b) = 0, \ M_2(x,0) = M_2(x,b) = 0$$
$$\psi_y(0,y) = \psi_y(a,y) = 0, \ M_1(0,y) = M_1(a,y) = 0$$

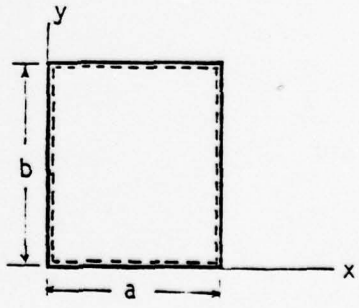

Loading (sinusoidal)

$$P_3=\bar{P}_3^{mn} \sin \alpha x \sin \beta y,\ T_o=\bar{T}_o^{mn} \sin \alpha x \sin \beta y,\ T_1=\bar{T}_1^{mn} \sin \alpha x \sin \beta y$$
$$P_1=\bar{P}_1^{mn} \sin \alpha x \cos \beta y\ ,\ P_2=\bar{P}_2^{mn} \cos \alpha x \sin \beta y\ ,\ \alpha = m\pi/a\ ,\ \beta = n\pi/b \tag{15}$$

and m and n are integers.

Plate construction (cross-ply, i.e., θ_m should be either 0° or 90°)

$$A_{16} = A_{26} = A_{45} = 0\ ,\ B_{16} = B_{26} = 0\ ,\ D_{16} = D_{26} = 0\ ,\ \alpha_6 = 0 \tag{16}$$

Under these specific conditions, the solution $(u_o, v_o, w, \psi_x, \psi_y)$ to Eq. (11) is of the form,

$$u_o = U_{mn} \cos \alpha x \sin \beta y\ ,\ v_o = V_{mn} \sin \alpha x \cos \beta y$$
$$w = W_{mn} \sin \alpha x \sin \beta y \tag{17}$$
$$\psi_x = X_{mn} \cos \alpha x \sin \beta y\ ,\ \psi_y = Y_{mn} \sin \alpha x \cos \beta y$$

where U_{mn}, V_{mn}, etc. are parameters to be determined subjected to the condition that the solution in Eq. (17) satisfies the operator equation (11) Substituting Eq. (17) into Eq. (11) we get

$$[C]\{\Delta\} = \{F\} \tag{18}$$

where

$$\{\Delta\} = \{U_{mn}, V_{mn}, W_{mn}, X_{mn}, Y_{mn}\}^T,\ \{F\} = \{\bar{F}_1^{mn}, \bar{F}_2^{mn}, \bar{F}_3^{mn}, \bar{F}_4^{mn}, \bar{F}_5^{mn}\}^T \tag{19}$$

and the elements of the coefficient matrix, [C], are given by

$$\begin{aligned}
&C_{11} = -A_{11}\alpha^2 - A_{66}\beta^2,\ C_{12} = -(A_{12} + A_{66})\alpha\beta \\
&C_{13} = 0,\ C_{14} = -\alpha^2 B_{11} - B_{66}\beta^2,\ C_{15} = -(B_{12} + B_{66})\alpha\beta \\
&C_{22} = -A_{22}\beta^2 - A_{66}\alpha^2,\ C_{23} = 0,\ C_{24} = C_{15}\ , \\
&C_{25} = -B_{22}\beta^2 - A_{66}\alpha^2,\ C_{33} = -\alpha^2 A_{55} - \beta^2 A_{44} \\
&C_{34} = -\alpha A_{55},\ C_{35} = -\beta A_{44},\ C_{44} = -D_{11}\alpha^2 - D_{66}\beta^2 - A_{55} \\
&C_{45} = -(D_{12} + D_{66})\alpha\beta\ ,\ C_{55} = -D_{66}\alpha^2 - D_{22}\beta^2 - A_{44}
\end{aligned} \tag{20}$$

$$\bar{F}_1^{mn} = \bar{P}_1^{mn} + \alpha[(A_{11}\alpha_1 + A_{12}\alpha_2)\,\bar{T}_o^{mn} + (B_{11}\alpha_1 + B_{12}\alpha_2)\,\bar{T}_1^{mn}\,]$$

$$\bar{F}_2^{mn} = \bar{P}_2^{mn} + \beta[(A_{12}\alpha_1 + A_{22}\alpha_2)\,\bar{T}_o^{mn} + (B_{12}\alpha_1 + B_{22}\alpha_2)\,\bar{T}_1^{mn}\,]$$

$$\bar{F}_4^{mn} = \alpha[(B_{11}\alpha_1 + B_{12}\alpha_2)\,\bar{T}_o^{mn} + (D_{11}\alpha_1 + D_{12}\alpha_2)\,\bar{T}_1^{mn}], \quad \bar{F}_3^{mn} = \bar{P}_3^{mn}$$

$$\bar{F}_5^{mn} = [(B_{12}\alpha_1 + B_{22}\alpha_2)\,\bar{T}_o^{mn} + (D_{12}\alpha_1 + D_{22}\alpha_2)\,\bar{T}_1^{mn}\,]$$

Thus, for a given $\alpha = m\pi/a$, $\beta = n\pi/b$, generalized forces $\bar{F}_i^{mn}$, and cross-ply construction, one needs to solve the 5 by 5 matrix equation (18) for the vector $\{\Delta\}$ of amplitudes of the generalized displacements.

Natural vibration frequencies ω can also be obtained for the boundary conditions and cross-ply construction discussed above by assuming a solution of the form (cf. Bert and Chen [15])

$$u_o = U(x,y)\cos\omega\tau\ ,\ v_o = V(x,y)\cos\omega\tau\ ,\ w = W(x,y)\cos\omega\tau$$
$$\psi_x = X(x,y)\cos\omega\tau\ ,\ \psi_y = Y(x,y)\cos\omega\tau \tag{21}$$

wherein $U(x,y)$, $V(x,y)$, etc. are the expressions in Eq. (17). Substituting Eq. (21) into Eq. (11) (with $P_1 = P_2 = P_3 = 0$, $T = 0$), we get the eigenvalue equation,

$$[C]\{\Delta\} = \omega^2[M]\{\Delta\} \tag{22}$$

where the elements $M_{ij} = M_{ji}$ of the mass matrix [M] are given by

$$M_{11} = M_{22} = M_{33} = R\ ,\ M_{14} = M_{25} = S\ ,\ M_{44} = M_{55} = I \tag{23}$$

and the remaining elements are zero.

B. Angle-Ply Plates in Bending and Vibration

Boundary conditions (simply supported edges)

$$u_o(0,y) = u_o(a,y) = 0\ ,\ N_6(0,y) = N_6(a,y) = 0$$
$$v_o(x,0) = v_o(x,b) = 0\ ,\ N_6(x,0) = N_6(x,b) = 0 \tag{24}$$
$$w(x,0) = w(x,b) = w(0,y) = w(a,y) = 0$$

$$\psi_x(x,0) = \psi_x(x,b) = 0 \ , \ M_2(x,0) = M_2(x,b) = 0$$
$$\psi_y(0,y) = \psi_y(a,y) = 0 \ , \ M_1(0,y) = M_1(a,y) = 0 \qquad \text{(24 cont.)}$$

Loading (sinusoidal)

$$P_1 = \bar{P}_1^{mn} \sin \alpha x \cos \beta y \ , \ P_2 = \bar{P}_2^{mn} \cos \alpha x \sin \beta y \ , \ P_3 = \bar{P}_3^{mn} \sin \alpha x \sin \beta y$$
$$T_o = \bar{T}_o^{mn} \cos \alpha x \cos \beta y \ , \ T_1 = \bar{T}_1^{mn} \sin \alpha x \sin \beta y \qquad (25)$$

Plate construction (antisymmetric angle-ply, $\theta/-\theta/\theta/-\theta$, ...)

$$A_{16} = A_{26} = A_{45} = 0 \ , \ B_{11} = B_{12} = 0 \ , \ D_{16} = D_{26} = 0 \ , \ \alpha_6 = 0 \qquad (26)$$

Then the solution to the associated boundary-value problem is of the form (multiply the functions with $\cos \omega\tau$ for eigenvalue problem)

$$u_o = U_{mn} \sin \alpha x \cos \beta y \ , \ v_o = V_{mn} \cos \alpha x \sin \beta y$$
$$w = W_{mn} \sin \alpha x \sin \beta y \qquad (27)$$
$$t\psi_x = X_{mn} \cos \alpha x \sin \beta y \ , \ t\psi_y = Y_{mn} \sin \alpha x \cos \beta y$$

where $\alpha = m\pi/a$ and $\beta = n\pi/b$, and m and n are integers. Substituting Eq. (27) into Eq. (11), we obtain,

$$[K]\{\Delta\} = \omega^2[M]\{\Delta\} + \{F\} \qquad (28)$$

where $\{\Delta\} = \{U_{mn}, V_{,m}, W_{,mn}, Y_{mn}, X_{mn}\}^T$, and

$$K_{11} = -(A_{11}\alpha^2 + A_{66}\beta^2) \ , \ K_{12} = -\alpha\beta(A_{12} + A_{66}) \ ,$$
$$K_{13} = 0 \ , \ K_{14} = -(\alpha^2 B_{16} + \beta^2 B_{26})/t, \ K_{15} = -2\alpha\beta B_{16}/t \ ,$$
$$K_{22} = -(\alpha^2 A_{66} + \beta^2 A_{22}) \ , \ K_{23} = 0 \ , \ K_{24} = -2\alpha\beta B_{26}/t$$
$$K_{25} = -(\alpha^2 B_{16} + \beta^2 B_{26})/t \ , \ K_{33} = -(\alpha^2 A_{55} + \beta^2 A_{44})$$
$$K_{34} = -\beta A_{44}/t \ , \ K_{35} = -\alpha A_{55}/t \ , \ K_{44} = -(\alpha^2 D_{66} + \beta^2 D_{22} + A_{44})/t^2$$
$$K_{45} = -\alpha\beta(D_{12} + D_{66})/t^2 \ , \ K_{55} = -(\alpha^2 D_{11} + \beta^2 D_{66} + A_{55})/t^2$$

The elements of the mass matrix, [M] are as defined in Eq. (23), and the elements of the force vector are given by

$$
\begin{aligned}
F_1 &= -\alpha\,(A_{11}\alpha_1 + A_{12}\alpha_2)T_0 + \beta(B_{16}\alpha_1 + B_{26}\alpha_2)T_1 \\
F_2 &= -\beta\,(A_{12}\alpha_1 + A_{22}\alpha_2)T_0 + \alpha(B_{16}\alpha_1 + B_{26}\alpha_2)T_1 \\
F_3 &= P_3/t \\
F_5 &= -\beta\,(B_{16}\alpha_1 + B_{26}\alpha_2)T_0 + \alpha(D_{11}\alpha_1 + D_{12}\alpha_2)T_1 \\
F_4 &= -\alpha\,(B_{16}\alpha_1 + B_{26}\alpha_2)T_0 + \beta(D_{12}\alpha_1 + D_{22}\alpha_2)T_1
\end{aligned}
\tag{29}
$$

FINITE-ELEMENT FORMULATION

As pointed out in the previous section, exact solution to Eq. (11) can be obtained only under special conditions of geometry, edge conditions, loadings, and lamination. Here we present a simple finite-element formulation which does not have any limitations (except for those implied in the formulation of the governing equations).

Suppose that the region R is subdivided into a finite number N of subregions or finite elements, R_e (e = 1,2,...,N). Over each element the generalized displacements $(u_o, v_o, w, \psi_x, \psi_y)$ are interpolated according to

$$
u_o = \sum_i^r u_i \phi_i^1 \,, \quad v_o = \sum_i^r v_i \phi_i^1 \,, \quad w = \sum_i^s w_i \phi_i^2 \,,
$$

$$
\psi_x = \sum_i^p \psi_{xi} \phi_i^3 \,, \quad \psi_y = \sum_i^p \psi_{yi} \phi_i^3 \tag{30}
$$

where ϕ_i^α (α = 1,2,3) is the interpolation function corresponding to the i-th node in the element. Note that the in-plane displacements, the transverse displacement, and the slope functions are approximated by different sets of interpolation functions. While this generality is included in the formulation (to indicate the fact that such independent approximations are possible),

we dispense with it in the interest of simplicity when the element is actually programmed and take $\phi_i^1 = \phi_i^2 = \phi_i^3$ ($r = s = p$). Here r, s, and p denote the number of degrees of freedom per each variable. That is, the total number of degrees of freedom per element is $2r + s + 2p$.

Substituting Eq. (30) into the Galerkin integrals associated with the operator equation (11), which must also hold in each element R_e,

$$\int_{R_e} ([L]\{\delta\} - \{f\})\{\phi\}\, dx\, dy = 0 \tag{31}$$

and using integration by parts once (to distribute the differentiation equally between the terms in each expression), we obtain

$$[K]\{\nabla\} = \omega^2 [M]\{\nabla\} + \{F\} \tag{32}$$

For static bending, Eq. (29) becomes

$$\begin{bmatrix} [K^{11}] & [K^{12}] & [0] & [K^{14}] & [K^{15}] \\ [K^{12}] & [K^{22}] & [0] & [K^{24}] & [K^{25}] \\ [0] & [0] & [K^{33}] & [K^{34}] & [K^{35}] \\ [K^{14}] & [K^{24}] & [K^{34}] & [K^{44}] & [K^{45}] \\ [K^{15}] & [K^{25}] & [K^{35}] & [K^{45}] & [K^{55}] \end{bmatrix}_e \begin{Bmatrix} \{u\} \\ \{v\} \\ \{w\} \\ \{\psi_x\} \\ \{\psi_y\} \end{Bmatrix}_e = \begin{Bmatrix} \{F^1\} \\ \{F^2\} \\ \{F^3\} \\ \{F^4\} \\ \{F^5\} \end{Bmatrix}_e \tag{33}$$

where the {u}, {v}, etc. denote the columns of the nodal values of u, v, respectively, and the elements $K_{ij}^{\alpha\beta}$ ($\alpha,\beta = 1,2,\ldots,5$) of the stiffness matrix and F_i^α of the force vector are given by

$$K_{ij}^{11} = A_{11}G_{ij}^x + A_{16}(G_{ij}^{xy} + G_{ji}^{xy}) + A_{66}G_{ij}^y$$

$$K_{ij}^{12} = A_{12}G_{ij}^{xy} + A_{16}G_{ij}^x + A_{26}G_{ij}^y + A_{66}G_{ji}^{xy}$$

$$K_{ij}^{14} = B_{11}H_{ij}^x + B_{16}(H_{ij}^{xy} + H_{ji}^{xy}) + B_{66}H_{ij}^y$$

$$K_{ij}^{15} = B_{12}H_{ij}^{xy} + B_{16}H_{ij}^{x} + B_{26}H_{ij}^{y} + B_{66}H_{ji}^{xy}$$

$$K_{ij}^{22} = A_{26}(G_{ij}^{xy} + G_{ji}^{xy}) + A_{22}G_{ij}^{y} + A_{66}G_{ij}^{x}$$

$$K_{ij}^{24} = B_{16}H_{ij}^{x} + B_{66}H_{ij}^{xy} + B_{12}H_{ji}^{xy} + B_{26}H_{ij}^{y}$$

$$K_{ij}^{25} = B_{26}(H_{ij}^{xy} + H_{ji}^{xy}) + B_{66}H_{ij}^{x} + B_{22}H_{ij}^{y}$$

$$K^{33} = A_{44}S_{ij}^{x} + A_{45}(S_{ij}^{xy} + S_{ji}^{xy}) + A_{55}S_{ij}^{y}$$

$$K^{34} = A_{44}R_{ij}^{xo} + A_{45}R_{ij}^{yo}\ ,\ K_{ij}^{35} = A_{45}R_{ij}^{xo} + A_{55}R_{ij}^{yo}$$

$$K_{ij}^{44} = D_{11}T_{ij}^{x} + D_{16}(T_{ij}^{xy} + T_{ji}^{xy}) + D_{66}T_{ij}^{y} + A_{44}T_{ij}^{o}$$

$$K_{ij}^{55} = D_{26}(T_{ij}^{xy} + T_{ji}^{xy}) + D_{66}T_{ij}^{x} + D_{22}T_{ij}^{y} + A_{55}T_{ij}^{o} \qquad (34)$$

$$M_{ij}^{\alpha\beta} = R \int_{R_e} \phi_i^{\alpha}\, \phi_j^{\beta}\ dx\ dy,\quad (\alpha = \beta = 1,2,3)$$

$$M_{ij}^{\alpha\beta} = S \int_{R_e} \phi_i^{\alpha}\, \phi_j^{\beta}\ dx\ dy \quad (\alpha,\beta = 4,5)$$

$$M_{ij}^{\alpha\beta} = T \int_{R_e} \phi_i^{\alpha}\, \phi_j^{\beta}\ dx\ dy \quad (\alpha = \beta = 4,5)$$

$$F_i^{\alpha} = \int_{R_e} f_{\alpha}\phi_i^{1}\ dx\ dy,\ (\alpha = 1,2;\ i = 1,2,\ldots,r)$$

$$F_i^{3} = \int_{R_e} q\phi_i^{2}\ dx\ dy,\ (i = 1,2,\ldots,s)$$

$$F_i^{\alpha} = \int_{R_e} f_{\alpha}\phi_i^{3}\ dx\ dy,\ (\alpha = 4,5;\ i = 1,2,\ldots,r)$$

where

$$G_{ij}^{\xi\eta} = \int_{R_e} \phi_{i,\xi}^{1}\, \phi_{j,\eta}^{1}\ dx\ dy\ ,\ (i,j = 1,2,\ldots,r)$$

$$H_{ij}^{\xi\eta} = \int_{R_e} \phi_{i,\xi}^{1}\, \phi_{j,\eta}^{3}\ dx\ dy\ ,\ (i = 1,2,\ldots,r;\ j = 1,2,\ldots,t) \qquad (35)$$

$$S_{ij}^{\xi\eta} = \int_{R_e} \phi_{i,\xi}^{2}\, \phi_{j,\eta}^{2}\ dx\ dy\ ,\ (i,j = 1,2,\ldots,s)$$

$$R_{ij}^{\xi\eta} = \int_{R_e} \phi_{i,\xi}^2 \, \phi_{j,\eta}^3 \, dx \, dy \, , \; (i = 1,2,\ldots,s; \; j = 1,2,\ldots,t)$$

$$T_{ij}^{\xi\eta} = \int_{R_e} \phi_{i,\xi}^3 \, \phi_{j,\eta}^3 \, dx \, dy \, , \; (i.j = 1,2,\ldots,t) \, , \; (\xi,\eta = 0,x,y)$$

and $G_{ij}^{xx} = G_{ij}^{x}$, etc. In the special case in which $\phi_i^1 = \phi_i^2 = \phi_i^3$, all of the matrices in Eq. (35) will coincide.

In the present study rectangular elements with four, eight, and nine nodes are employed with the same interpolation for all of the variables. The resulting stifness matrices are 20 by 20 for the 4-node element and 40 by 40 for the 8-node element. As pointed out in a recent study [6], the YNS theory can be derived from the corresponding classical thin-plate theory by treating the slope-displacement relations

$$\frac{\partial w}{\partial x} = -\theta_x \, , \; \frac{\partial w}{\partial y} = -\theta_y \tag{36}$$

as constraints. Indeed, when the constraints in Eq. (36) are incorporated into the classical thin-plate theory by means of the penalty method, the resulting equations correspond to the YNS theory with the correspondence,

$$\theta_x \sim \psi_x \text{ and } \theta_y \sim \psi_y \tag{37}$$

It is now well-known that whenever the penalty method is used, the so-called reduced integration [9] must be used to evaluate the matrix coefficients in Eq. (34). That is, if the four-node rectangular element is used, the 1 x 1 Gauss rule must be used in place of the standard 2 x 2 Gauss rule to numerically evaluate the coefficients K_{ij}.

NUMERICAL RESULTS

In the following, we present numerical results for bending and vibration analyses of laminated anisotropic plates. In most of the problems considered here the following two sets of material properties were employed:

$$\begin{aligned} &\text{Material I:} \quad E_1/E_2 = 25,\ G_{12}/E_2 = 0.5,\ G_{23}/E_2 = 0.2,\ \nu_{12} = 0.25 \\ &\text{Material II:} \quad E_1/E_2 = 40,\ G_{12}/E_2 = 0.6,\ G_{23}/E_2 = 0.5,\ \nu_{12} = 0.25 \end{aligned} \tag{38}$$

Further, it was assumed that $G_{12} = G_{23}$ and $\nu_{12} = \nu_{13}$. A value of 5/6 was used for the shear correction coefficients, $k_1^2 = k_2^2$ (see Whitney [11]). The thermal properties (i.e., coefficients of thermal expansion, α_i) are given during the discussion of the results. All of the computations were carried on an IBM 370/158 computer.

Bending Analysis

Numerical experiments were conducted to investigate the effect of element type (i.e., linear, eight-node quadratic, and nine-node quadratic), mesh (L2 = linear 2 by 2, Q2 = 2Q8 = 8-node quadratic 2 by 2 elements in quarter plate), and reduced integration on the deflections, stresses, and natural frequencies. In some cases the difference is not distinct enough to show on the graph, therefore the results are presented in tabular form. Table 1 shows the effect of the element type, mesh, and reduced integration on the accuracy of the maximum deflection and stresses (also see Fig. 1).

In Table 1 linear and quadratic elements are compared for deflections and stresses of a three-layer ($t_1=t_3=t/4$, $t_2=t/2$) square plate (Material I) subjected to sinusoidal loading. This problem is also equivalent to a four-layer (equal thickness) cross-ply. The stresses were computed at the Gaussian points:

Table 1 Effect of reduced integration on the maximum deflection and stresses of three-ply (0°/90°/0°) square plate subjected to sinusoidal loading ($t_1=t_3=t/4$, $t_2=t/2$).

	Source		$\bar{w}$	$\bar{\sigma}_x$	$\bar{\sigma}_y$	$\bar{\tau}_{xy}$	$\bar{\tau}_{xz}$	$\bar{\tau}_{yz}$
10	CFS		7.0680	0.4925	0.3763	0.0246	0.418	0.128
	Finite-Element Solution	4L-R	6.5986	0.4668	0.3466	0.0227	0.395	0.2078
		4L-F	6.4267	0.4512	0.3280	0.0219	347.5	347.2
		2Q8-R	6.6152	0.4842	0.3509	0.0234	0.404	0.1255
		2Q8-F	6.6047	0.4831	0.3492	0.0234	370.5	370.2
		2Q9-R	6.5610	0.4800	0.3410	0.0231	0.400	0.126
		2Q9-F	6.5510	0.4790	0.3400	0.0231	0.399	0.126
		2Q9-FR	6.5580	0.4800	0.3410	0.0230	0.400	0.126
		2L-R	6.5079	0.3799	0.2838	0.0187	0.335	0.1067
		2L-F	5.9011	0.3339	0.2454	0.0163	261.6	261.4
20	CFS		5.0300	0.5252	0.3005	0.0223	0.434	0.108
	Finite-Element Solution	4L-R	4.8633	0.4940	0.2777	0.0207	0.415	0.1034
		4L-F	4.3461	0.4365	0.2451	0.0183	115.5	115.25
		2Q8-R	4.0914	0.5112	0.2870	0.0214	0.424	0.1057
		2Q8-F	4.8764	0.5082	0.2837	0.0214	134.5	134.25
		2Q9-R	4.8470	0.5050	0.2780	0.0213	0.418	0.106
		2Q9-F	4.8270	0.5020	0.2750	0.0211	0.418	0.107
		2Q9-FR	4.8470	0.5050	0.2780	0.0212	0.417	0.106
		2L-R	4.7117	0.4037	0.2289	0.0170	0.3529	0.0886
		2L-F	3.2355	0.2645	0.1490	0.0111	70.55	70.4

(Table 1 continued)

50	CFS		4.4290	0.5364	0.2746	0.0214	0.441	0.101
	Finite-Element Solution	4L-R	4.3547	0.5032	0.2566	0.0201	0.421	0.0967
		4L-F	2.4475	0.2792	0.1424	0.0111	17.846	17.668
		2Q8-R	4.3979	0.5208	0.2655	0.0208	0.432	0.1000
		2Q8-F	4.3098	0.5056	0.2540	0.0204	32.48	32.18
		2L-R	4.1837	0.4116	0.2103	0.0164	0.359	0.0825
		2L-F	1.0493	0.0975	0.0499	0.0039	6.402	6.34
100	CFS		4.3420	0.5381	0.2707	0.0213	0.442	0.1001
	Finite-Element Solution	4L-R	4.2811	0.5045	0.2535	0.0200	0.422	0.0958
		4L-F	1.0339	0.1203	0.0604	0.0048	9.327	9.404
		2Q8-R	4.3192	0.5214	0.2621	0.0206	0.435	0.1020
		2Q8-F	4.1425	0.4900	0.2435	0.0199	39.77	40.13
		2Q9-R	4.3006	0.5180	0.2550	0.0207	0.428	0.0989
		2Q9-F	4.1580	0.4900	0.2420	0.0201	0.427	0.0996
		2Q9-FR	4.2990	0.5180	0.2550	0.0206	0.426	0.0985
		2L-R	4.1072	0.4129	0.2076	0.0164	0.356	0.08163
		2L-F	0.3149	0.0299	0.0151	0.0012	2.173	2.192

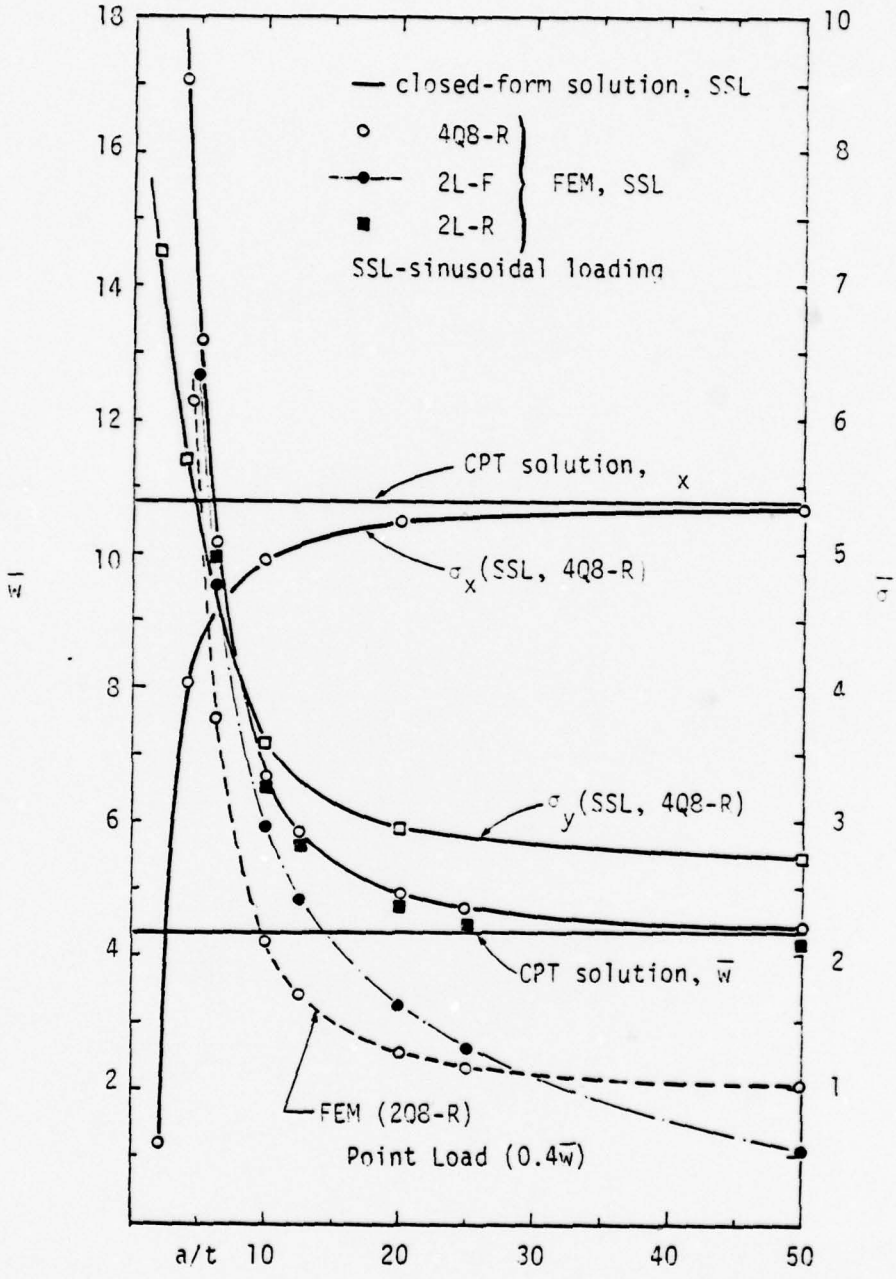

Figure 1 Closed-form and finite-element solutions for simply-supported four-layer cross-ply (0°/90°/90°/0°) square plate (Material I)

$$\bar{w} = \frac{w(\frac{a}{2},\frac{a}{2},0)\ E_2 t^3 \times 10^3}{q_o a^4} \quad , \quad \bar{\sigma}_x = (\frac{t}{a})^2 \frac{1}{q_o} \sigma_x(A,A,\pm t/2),\ q_o = P_3$$

$$\bar{\sigma}_y = (\frac{t}{a})^2 \frac{1}{q_o} \sigma_y(A,A,\pm t/4) \quad , \quad \bar{\tau}_{xy} = (\frac{t}{a})^2 \frac{1}{q_o} \tau_{xy}(B,B,\pm t/2) \qquad (39)$$

$$\bar{\tau}_{xz} = \frac{t}{aq_o} \tau_{xz}(B,A) \text{ in layers 1 \& 3; } \bar{\tau}_{yz} = \frac{t}{aq_o} \tau_{yz}(A,B) \text{ in layer 2}$$

where A and B are the Gauss-point coordinates (as a fraction of sides a and b) given below:

	2x2 linear	4x4 linear	2x2 quadratic	4x4 quadratic
A	0.125	0.0625	0.05283	0.02642
B	0.375	0.4375	0.4472	0.4736

In Table 1, R denotes reduced integration, F = full integration, and FR = full integration for bending terms, and reduced integration for the shear terms. The following observations can be made from the results of Table 1.

1. The nine-node element gives virtually the same results for full (3x3 Gauss rule), reduced (2x2 Gauss rule), and mixed (3x3 and 2x2 Gauss rules) integrations. However, the results attained by using the reduced integration are the closest of all three integrations to the closed-form solution (CFS).
2. The nine-node element and the eight-node element (with reduced integration) give almost identical results (contrary to the belief that the nine-node element is superior to the eight-node element) for all side-to-thickness ratios. In fact, the eight-node element is relatively more accurate.

3. Integration rule has a more profound effect on the accuracy in the eight-node element than in the nine-node element. Full integration gives less accurate results than the reduced integration, and the error increases with the side-to-thickness ratio. This implies that the reduced integration is a must for thin plates, as generally recognized for all penalty models.
4. Full integration results in, relatively, smaller errors for quadratic elements and for refined meshes than for linear elements and/or for coarse meshes. That is, the error between the solutions obtained by 2Q8-F and 2Q8-R is smaller than those obtained by 4L-F and 4L-R, and the error between the solutions obtained by 4L-F and and 4L-R is smaller than those obtained by 2L-F and 2L-R.
5. Numerical convergence of the element is clear from the results (see also Table 2 for 4Q8 results).

In the results to be presented, reduced integration was used with linear and eight-node quadratic elements.

In Table 2, 3-D elasticity solution (3-DES) of Pagano and Hatfield [12], the present closed-form solution (CFS) and 4Q8 finite-element results (FEM), and the finite-element results of Panda and Natarajan [8] are compared for the problem discussed in Table 1. The present finite-element results are in excellent agreement with the closed-form solution of the equations governing the YNS theory. The stresses in 3-D elasticity solution were reported to be maximum at the following points:

$$\bar{\sigma}_x = \bar{\sigma}_x(\tfrac{a}{2},\tfrac{b}{2},\pm t/2) \quad , \quad \bar{\sigma}_y = \bar{\sigma}_y(\tfrac{a}{2},\tfrac{b}{2},\pm t/4) \quad , \quad \bar{\tau}_{xy} = \bar{\tau}_{xy}(a,b,\tfrac{t}{2})$$
$$\bar{\tau}_{xz} = \bar{\tau}_{xz}(a,\tfrac{b}{2},0) \quad , \quad \bar{\tau}_{yz} = \bar{\tau}_{yz}(\tfrac{a}{2},b,0) \tag{40}$$

Table 2 Comparison of maximum deflection and stresses in three-ply (0°/90°/0°) square plate subjected to sinusoidal loading ($t_1=t_3=t/4$, $t_2 = t/2$, Material I, 4Q8-R element)

a/t	source	$\bar{w}$	$\bar{\sigma}_x$	$\bar{\sigma}_y$	$\bar{\tau}_{xy}$	$\bar{\tau}_{xz}$	$\bar{\tau}_{yz}$
2	3-DES	51.189	1.338	0.835	0.863	0.153	0.295
	CFS	50.625	0.337	0.725	0.353	0.1198* (0.2995)	0.242
	FEM	50.623	0.337	0.725	0.353	0.120 (0.299)	0.2227
4	3-DES	19.537	0.720	0.663	0.467	0.219	0.292
	CFS	17.094	0.403	0.572	0.306	0.1388 (0.347)	0.195
	FEM	17.094	0.403	0.572	0.306	0.1388 (0.3472)	0.195
10	3-DES	7.434	0.559	0.403	0.276	0.301	0.196
	CFS	6.627	0.496	0.359	0.240	0.166 (0.414)	0.128
	FEM	6.627	0.495	0.359	0.240	0.165 (0.414)	0.128
	Ref. [8]	6.299	0.532	0.307	0.250	--	--
20	3-DES	5.173	0.543	0.308	0.230	0.328	0.156
	CFS	4.911	0.524	0.294	0.219	0.174 (0.434)	0.108
	FEM	4.911	0.524	0.294	0.219	0.174 (0.434)	0.108
	Ref. [8]	4.847	0.557	0.307	0.231	--	--
50	3-DES	4.485	0.539	0.276	0.216	0.337	0.141
	CFS	4.410	0.533	0.272	0.213	0.176 (0.441)	0.101
	FEM	4.410	0.533	0.272	0.213	0.176 (0.441)	0.101
	Ref. [8]	4.421	0.565	0.287	0.225	--	--
100	3-DES	4.385	0.539	0.271	0.214	0.339	0.139
	CFS	4.337	0.535	0.269	0.212	0.177 (0.442)	0.1001
	FEM	4.336	0.535	0.269	0.212	0.177 (0.442)	0.1002
	Ref. [8]	4.363	0.566	0.284	0.223	--	--
classical thin-plate solution		4.350	0.539	0.269	0.213	0.339	0.138

*First value is in the center layer, and the value in parenthesis is in the top and bottom layers.

Note that the present finite-element solutions cannot be expected to agree well with the 3-D elasticity solution since the element is based on the YNS theory rather than the 3-D elasticity equations. The accuracy of the YNS theory is evident from the results. While the YNS theory seems to predict the maximum deflection very close to that given by the 3-D elasticity solution, the stresses, especially the transverse shear stresses, are not in good agreement for thick plates. The stresses predicted by the YNS theory are on the lower side of the 3-D elasticity results.

Table 3 shows a comparison of the 'exact' solution of Pagano [13], with the present closed-form solution and finite-element results for a three-layer (equal thickness) cross-ply square plate (Material I). Again, the results are in good agreement with the 'exact' solution. Table 4 shows similar results for a rectangular plate (b/a = 3) of the same construction as above. The present element gives more accurate results compared to those obtained by Panda and Natarajan [8], who used a complicated shell element in their analysis.

Deflection and stresses are compared in Table 5 for five-layer ($t_1=t_3=t_5=t/6$, $t_2=t_4=t/4$) cross-ply (0°/90°/0°/90°/0°) square plate (Material I) under sinusoidal loading. While the finite-element solution is close to the closed-form solution, the YNS theory gives, relatively, less accurate solutions for the five-layer case compared to the three-layer case shown in Table 2.

Table 6 compares the maximum deflection and stresses in a three-layer ($t_1=t_3=0.1t$, $t_2=0.8t$), sandwich square plate (0°/90°/0°) subjected to sinusoidal loading. The material of the face sheets (i.e., layers 1 and 3) is the same as Material I, and the core material is transversely isotropic with respect to z and is characterized by the following properties (see Pagano [13]),

Table 3. Comparison of maximum deflection and stresses for three-ply (0°/90°/0°) square plate subected to sinusoidal loading (t_i =t/3, Material I).

a/t	Source		$0.1\bar{w}$	$\bar{\sigma}_x$	$\bar{\sigma}_y$	$\bar{\tau}_{xy}$	$\bar{\tau}_{xz}$	$\bar{\tau}_{yz}$
10	Pagano [13]		-	0.590	0.288	0.029	0.357	0.123
	closed-form solution		0.669	0.510 0.499	0.252 0.247	0.0250 0.0243	0.406 0.396	0.091* 0.089
	Present FEM	4Q8-R	0.669	0.510	0.252	0.0250	0.406	0.091
		2Q8-R	0.668	0.498	0.246	0.0244	0.397	0.089
20	Pagano [13]		-	0.552	0.210	0.0234	0.385	0.094
	closed-form solution		0.482	0.528 0.517	0.198 0.194	0.0222 0.0216	0.418 0.408	0.075 0.074
	FEM	4Q8-R	0.492	0.528	0.198	0.0222	0.418	0.075
		2Q8-R	0.491	0.516	0.194	0.0217	0.408	0.074
50	Pagano [13]		-	0.541	0.185	0.0216	0.393	0.084
	closed-form solution		0.441	0.534 0.523	0.182 0.178	0.0213 0.0207	0.421 0.412	0.071 0.069
	FEM	4Q8-R	0.441	0.534	0.182	0.0213	0.421	0.071
		2Q8-R	0.440	0.521	0.178	0.0208	0.412	0.070
100	Pagano [13]		-	0.539	0.181	0.0213	0.395	0.083
	closed-form solution		0.434	0.535 0.524	0.179 0.176	0.0212 0.0206	0.422 0.412	0.0 0.068
	FEM	4Q8-R	0.434	0.535	0.179	0.0212	0.422	0.070
		2Q8-R	0.432	0.522	0.175	0.0207	0.416	0.068
classical plate theory [3]			-	0.539	0.180	0.0213	0.395	0.082

* The first row of stresses is for 4x4 Gauss points and the second row is for 2x2 Gauss points.

Table 4 Comparison of maximum deflection and stresses in three-ply (0°/90°/0°) rectangular (b=3a) plate subjected to sinusoidal loading (t_i=t/3, Material I, 4Q8-R)

a/t	Source	$\bar{w}$	$-\bar{\sigma}_x$	$-\bar{\sigma}_y$	$\bar{\tau}_{xy}$	$\bar{\tau}_{xz}$	$\bar{\tau}_{yz}$
2	3-D elasticity [13]	8.17	1.62	0.268	0.0548	0.455	0.0668
	closed-form sol.	7.82	0.590	0.218	0.0427	0.458	0.0639
	present FEM	7.82	0.590	0.218	0.0427	0.458	0.0638
4	3-D elasticity [13]	2.82	1.10	0.119	0.0281	0.387	0.0334
	closed-form	2.36	0.607	0.0928	0.0203	0.467	0.0306
	present FEM	2.36	0.607	0.093	0.0203	0.467	0.0299
10	3-D elasticity [13]	0.919	0.725	0.0435	0.0123	0.420	0.0152
	closed-form	0.863	0.617	0.0372	0.0104	0.470	0.0158
	FEM	0.863	0.617	0.0372	0.0104	0.470	0.0158
	Panda & Natarajan[8]	0.752	0.653	0.0367	0.0105	--	--
20	3-D elasticity [13]	0.610	0.650	0.0299	0.0093	0.434	0.0119
	closed-form	0.578	0.619	0.0281	0.00878	0.471	0.0134
	FEM	0.578	0.619	0.0281	0.0088	0.471	0.0134
	Panda & Natarajan[8]	0.565	0.654	0.0287	0.0091	--	--
50	3-D elasticity [13]	0.520	0.628	0.0259	0.0084	0.439	0.0110
	closed-form	0.515	0.619	0.0255	0.00831	0.471	0.0127
	FEM	0.515	0.619	0.0255	0.00831	1.471	0.0127
	Panda & Natarajan[8]	0.513	0.654	0.0264	0.0087	--	--
100	3-D elasticity [13]	0.508	0.624	0.0253	0.0083	0.439	0.0108
	closed-form	0.506	0.619	0.251	0.00825	0.471	0.0126
	FEM	0.506	0.619	0.0251	0.00825	0.471	0.0126
	Panda & Natarajan	0.505	0.654	0.0261	0.0086	--	--
classical thin plate solution		0.503	0.623	0.0252	0.0083	0.440	0.0108

Table 5 Comparison of maximum deflection and stresses for five-layer (0°/90°/0°/90°/0°) square plate under sinusoidal loading ($t_1 = t_3 = t_5 = t/6$, $t_2 = t_4 = t/4$, Material I, 2Q8-R).

a/t	source	$\bar{w}$	$\pm\bar{\sigma}_x$	$\pm\bar{\sigma}_y$	$-\bar{\tau}_{xy}$	$\bar{\tau}_{xz}$	$\bar{\tau}_{yz}$
2	3-DES+[13]	53.415	1.332	1.001	0.0836	0.227	0.186
	CFS	48.35	0.391	0.537	0.0235	0.275	0.102* (0.254)
	FEM	48.292	0.3902	0.5355	0.0236	0.275	0.102 (0.254)
4	3-DES [13]	18.668	0.685	0.633	0.0394	0.238	0.229
	CFS	15.623	0.425	0.489	0.0227	0.296	0.0932 (0.2330)
	FEM	15.602	0.4241	0.4879	0.0228	0.296	0.0933 (0.2334)
10	3-DES [13]	6.830	0.545	0.430	0.0246	0.258	0.223
	CFS	6.213	0.488	0.400	0.0214	0.335	0.0775 (0.1942)
	FEM	6.201	0.487	0.397	0.0214	0.336	0.0776 (0.194)
20	3-DES [13]	4.981	0.539	0.380	0.0222	0.268	0.212
	CFS	4.796	0.513	0.365	0.0208	0.351	0.0714 (0.1788)
	FEM	4.786	0.512	0.364	0.0209	0.351	0.0715 (0.1788)
50	3-DES [13]	4.451	0.539	0.363	0.0214	0.271	0.206
	CFS	0.522	0.522	0.352	0.0206	0.356	0.0692 (0.173)
	FEM	4.379	0.521	0.351	0.0207	0.357	0.0696 (0.1741)
100	3-DES [13]	4.377	0.539	0.360	0.0213	0.272	0.205
	CFS	4.332	0.524	0.350	0.0206	0.357	0.0688 (0.172)
	FEM	4.314	0.521	0.347	0.0206	0.361	0.0705 (0.176)
CPT		4.3505	0.539	0.359	0.0213	0.272	0.205

+ 3-DES - 3-D elasticity solution

*First value is in layers 1,3,and 5 and the value in parenthesis is in layers 2 and 4.

Table 6. Comparison of maximum deflection and stresses in a three-layer sandwich (0°/90°/0°) plate subjected to sinusoidal loading ($t_1=t_3=0.1t$, $t_2=0.8t$, Material I, 2Q8-R).

a/t	source	$\bar{w}$	$\bar{\sigma}_x$	$\bar{\sigma}_y$	$\bar{\tau}_{xy}$	$\bar{\tau}_{xz}$	$\bar{\tau}_{yz}$
2	3-DES[13]	-	3.278	0.4517	0.2403	0.185	0.140
	CFS	9.552	1.148	0.3622	0.1954	0.876	0.252
	FEM	9.543	1.145	0.3615	0.1961	0.877	0.253
4	3-DES[13]	-	1.556	0.2595	0.1437	0.239	0.107
	CFS	4.7672	0.867	0.1520	0.0877	0.993	0.174
	FEM	4.7606	0.865	0.1517	0.8806	0.994	0.174
10	3-DES[13]	-	1.153	0.1104	0.0707	0.300	0.053
	CFS	1.560	1.017	0.0776	0.0533	1.110	0.095
	FEM	1.5578	1.015	0.0774	0.0535	1.112	0.095
20	3-DES[13]	-	1.110	0.0700	0.0511	0.317	0.036
	CFS	1.0524	1.053	0.0595	0.0450	1.140	0.076
	FEM	1.0503	1.051	0.0594	0.0452	1.140	0.076
50	3-DES[13]	-	1.064	0.0541	0.0425	0.323	0.031
	CFS	0.9064	1.065	0.0539	0.0424	1.148	0.070
	FEM	0.9040	1.062	0.0538	0.0425	1.151	0.071
100	3-DES[13]	-	1.098	0.0550	0.0437	0.324	0.0297
	CFS	0.8852	1.067	0.0531	0.0420	1.149	0.069
	FEM	0.8822	1.063	0.0530	0.0421	1.158	0.072
	CPT	-	1.097	0.0534	0.0433	0.324	0.0295

Table 7 Nondimensionalized deflection as a function of number of layers, angle, and side-to-thickness ratio for simply-supported angle-ply square plate (Material II, 2Q8-R)

a/t	Source	θ = 5°		θ = 30°		θ = 45°	
		n = 2	n = 16	n = 2	n = 16	n = 2	n = 16
2	CFS	37.850	36.840	33.325	29.878	32.300	29.131
	FEM	37.106	36.824	31.117	29.860	30.474	29.111
4	CFS	13.164	12.596	12.155	8.875	11.575	8.429
	FEM	12.866	12.578	10.152	8.855	9.722	8.407
5	CFS	9.760	9.256	9.568	6.316	9.088	5.938
	FEM	9.536	9.238	7.598	6.297	7.210	5.922
6.25	CFS	7.475	7.008	7.909	4.669	7.496	4.346
	FEM	7.302	6.994	5.946	4.652	5.586	4.332
10	CFS	4.883	4.454	6.099	2.872	5.773	2.621
	FEM	4.764	4.447	4.114	2.859	3.776	2.609
12.5	CFS	4.264	3.843	5.678	2.456	5.376	2.224
	FEM	4.156	3.836	3.672	2.443	3.334	2.211
20	CFS	3.585	3.172	5.224	2.005	4.944	1.793
	FEM	3.487	3.165	3.163	1.992	2.814	1.781
25	CFS	3.427	3.015	5.119	1.900	4.844	1.693
	FEM	3.330	3.008	3.032	1.888	2.676	1.681
50	CFS	3.215	2.806	4.979	1.761	4.711	1.560
	FEM	3.119	2.800	2.815	1.748	2.440	1.548
100	CFS	3.162	2.754	4.944	1.726	4.678	1.527
	FEM	3.065	2.742	2.725	1.712	2.335	1.514

$$E_1/E_2 = 1.0 \quad , \quad E_3/E_2 = 12.5 \quad \text{(not used in the YNS theory)}$$
$$G_{13}/G_{23} = 1.5E_2 \quad , \quad G_{12} = 0.4\ E_2 \quad , \quad \nu_{12} = \nu_{13} = \nu_{23} = 0.25 \tag{41}$$

The finite-element results are in good agreement with the closed-form solution; however, the YNS theory seems to predict the stresses quite low for thick plates.

A comment is in order on the closed-form solutions for the cross-ply and angle-ply plates subjected to sinusoidal loadings and edge conditions given in equations (14) and (24). In the case of cross-ply plates the assumed solution in (17) and (21) satisfies, in addition to the boundary conditions in (14), the following boundary conditions,

$$N_1(x,0) = N_1(x,b) = 0;\ N_2(0,y) = N_2(a,y) = 0 \tag{42}$$

Similarly, in the case of angle-ply plates, the following additional boundary conditions are satisfied by the solution in (27):

$$M_1(x,0) = M_1(x,b) = 0\ ,\ M_2(0,y) = M_2(a,y) = 0 \tag{43}$$

From the variational formulation of the equations in (1)-(7), it follows that the only boundary conditions that are physical and mathematically correct are those in (14) and (24). That is, for example, if u is specified (essential boundary condition) at a boundary, N_1 cannot be specified (natural boundary condition) there, and vice versa. Similarly, if ψ_x is specified at a boundary then M_1 cannot be specified there. Indeed, in the finite-element formulation it is not possible, even if we wish, to specify the essential and natural boundary conditions on the same portion of the boundary. As a result, there seems to exist an inherent difference between the closed-form solutions and finite-element solutions. However, from the

cross-ply bending results it is clear that this difference is not noticeable. The reason could be attributed to the fact that the additional boundary conditions (42) are also nearly met by the finite element solution. This is due to the fact that the in-plane displacements are zero everywhere in the plate, and there are very small in-plane forces in the plate (i.e., N_1 and N_2 are almost zero everywhere in the plate). However, for thermal loading, N_1 and N_2 are even larger (although small), and the results may not agree as closely as seen thus far.

The additional boundary conditions (43), in the case of angle-ply plates, are too severe to be satisfied by the finite-element method in all cases. The bending moments are typically large, and their magnitude decreases with the stiffness coefficients, B_{16} and B_{26}. These coefficients are large for an even number of layers and their magnitude decreases with increasing number of layers (see Tsai [14]). Thus, in angle-ply plates the finite-element solutions and the closed-form solutions could differ substantially for small number of layers (say n = 2) and be almost equal for large number of layers ($n \to \infty$).

One other comment that applies to the closed-form solution (27) of angle-ply plates is that the assumed solution forces u and v to vanish at y = b/2 and x = a/2, respectively:

$$u(x,b/2) = 0 \ , \quad v\ (a/2,y) = 0 \tag{44}$$

In the finite-element modeling of a quarter plate, the following symmetry conditions were used for all edge conditions and laminations:

$$u(a/2,y) = 0,\ \psi_x(a/2,y) = 0,\ v(x,b/2) = 0,\ \psi_y(x,b/2) = 0 \tag{45}$$

Clearly, the symmetry boundary conditions in (45) are physical whereas those in (44) are not physically meaningful. This marks another difference (which turns out to be a major one) between the closed-form and finite-element formulations. Of course, one can force the symmetry boundary conditions (44) in the finite-element model. Indeed, when the symmetry conditions in (44) are forced, the finite-element solution satisfies the boundary conditions in (43), and consequently the two solutions agree very closely.

The above observations are supported by the numerical results obtained for the angle-ply plates. Table 7 shows the maximum nondimensionalized deflection for two- and sixteen-layer angle-ply ($\theta/-\theta/\theta/-\theta,\ldots$) square plate (Material II) under sinusoidal loading. Since the stiffness coefficient B_{16} ($\sim 1/n$) is the largest at $\theta = 45°$ for a given even number of layers, it is the worst case in terms of the agreement with the closed-form solution. However, for n = 16, the finite-element solution is in good agreement with the closed-form solution. As expected, the results for $\theta = 5°$ and $30°$ are closer to the closed-form solution, even for n = 2, compared to the results obtained for $\theta = 45°$.

Figure 2 shows the effect of side-to-thickness ratio (a/t), number of layers, lamination angle, and the symmetry boundary conditions on the nondimensionalized maximum deflection. Note that for $\theta = 45°$, the finite-element solution obtained with the physical boundary conditions in (45) is about one-half of the closed-form solution for n = 2, whereas for n = 16 they are almost identical. When the symmetry boundary conditions in (44) are employed, instead of those in (45), in the finite-element model, the closed-form and finite-element solutions are in excellent agreement for any n and θ (Figure 2 contains results only for n = 4 and $\theta = 45°$).

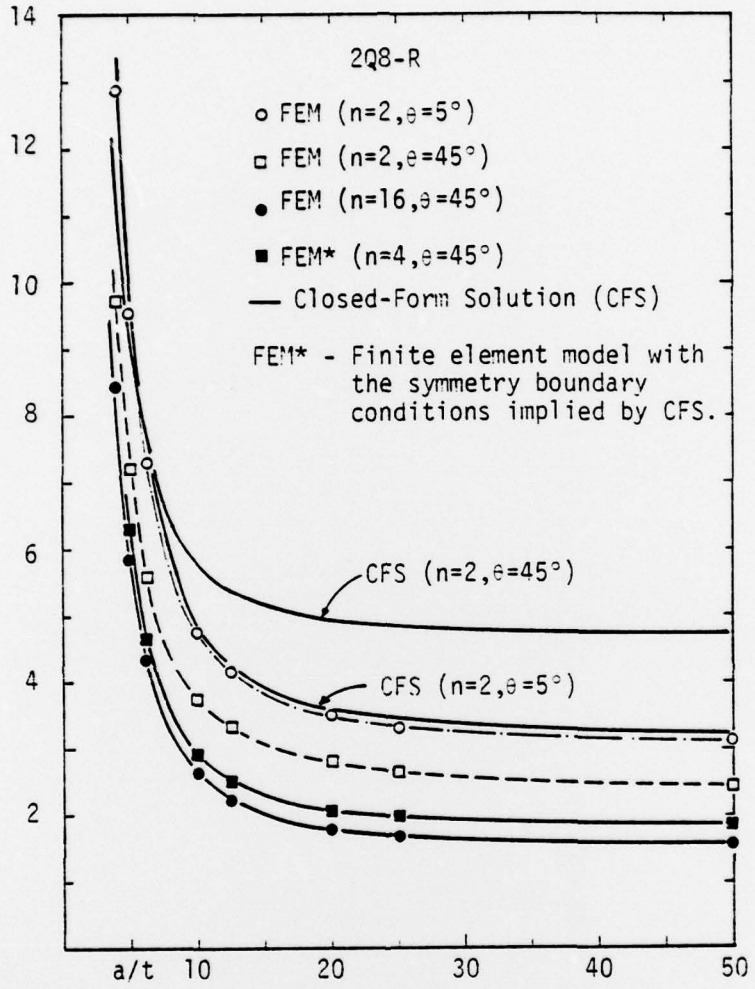

Figure 2 Effect of side-to-thickness ratio, number of layers, lamination angle, and the symmetry boundary conditions on the nondimensionalized deflection of an angle-ply square plate (Material II).

Figure 3 shows the nondimensionalized deflection versus the lamination angle for two, four and sixteen layer angle-ply (0/-0/0/-0/.../) square plates (Material II) under sinusoidal loading. Dark lines and symbols correspond, respectively, to the closed-form solution and the finite-element solution with the symmetry conditions of the CFS imposed. They are in excellent agreement with each other. The broken lines in Figure 3 correspond to the finite-element solution obtained by using the physically appropriate symmetry boundary conditions. Open symbols are used for thick plates (a/t = 10) and dark symbols are used for thin (a/t = 100) plates.

Table 8 shows the nondimensionalized deflection as a function of side-to-thickness ratio, element type and mesh for a cross-ply (0°/90°/0°, t_i=t/3) plate (Material I with $\alpha_2 = 3\alpha_1$) under sinusoidal temperature distribution. The finite-element results are in excellent agreement with the closed-form solution. Figure 4 shows the effect of side-to-thickness ratio (a/t) on the nondimensionalized deflection and stresses for cross-ply and angle-ply plates subjected to thermal loading (P_i = 0). The scale for the deflection and stresses is amplified to show the effect of thickness-shear strain.

Free Vibration Analysis

Once again, the effect of reduced integration and the use of eight and nine node elements on the accuracy of the natural frequencies are studied using three-layer cross-ply (0°/90°/0°) example problem of Table 1. Table 9 shows the nondimensionalized fundamental natural frequency as a function of side-to-thickness ratio, type of integration, and type of element. From the results obtained, it is clear that no single integration type is the best choice (in contrast to the observations made in the bending analysis) for all ratios of side to thickness. However, the reduced integration still seems to be giving better results for most ratios of side to thickness.

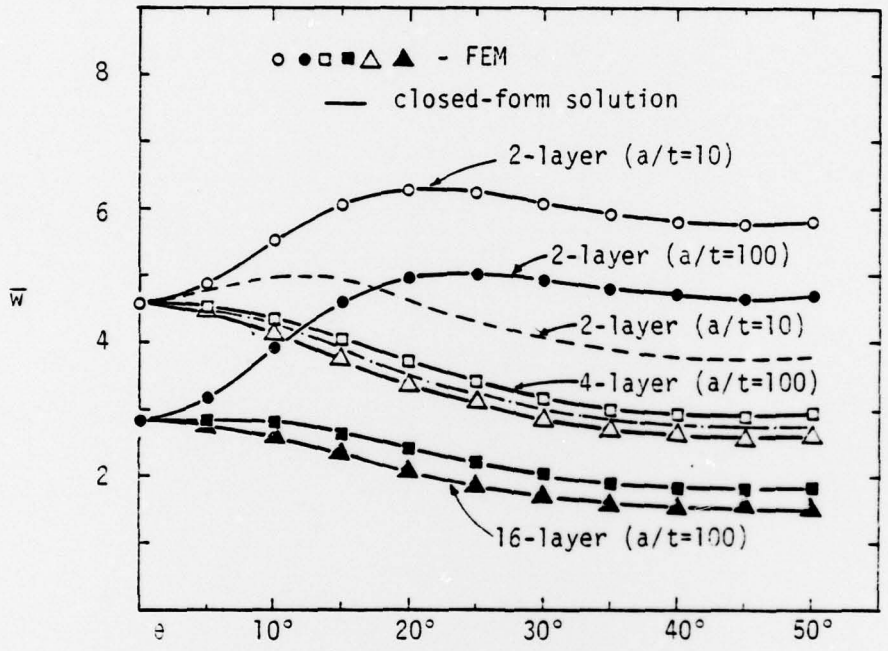

Figure 3. Nondimensionalized deflection versus the lamination angle (θ) for antisymmetric angle-ply square plates (Material II)

Table 8 Three-Layer (0°/90°/0°) Simply-Supported Square Plate (Material I, $\alpha_2 = 3\alpha_1$) Subjected to Sinusoidal Temperature Distribution

a/t	Source	Deflection $\bar{w} = w \frac{10h}{\alpha_1 T_1 a^2}$				
		a/b=1/3	a/b=0.5	a/b=1.0	a/b=1.5	a/b=2.0
100	FEM L2x2	1.1154	1.1311	1.1530	1.0369	0.80483
	FEM L4x4	1.0730	1.0880	1.1090	0.99741	0.77422
	FEM Q2x2	1.0617	1.0727	1.0917	0.98154	0.76206
	FEM Q4x4	1.0592	1.0740	1.0948	0.98458	0.76427
	CFS	1.0593	1.0741	1.0949	0.9847	0.7643
50	FEM L2x2	1.1158	1.1319	1.1546	1.0374	0.80416
	FEM L4x4	1.0733	1.0887	1.1105	0.99790	0.77362
	FEM Q2x2	1.0604	1.0740	1.0947	0.98358	0.76259
	FEM Q4x4	1.0595	1.0747	1.0962	0.98506	0.76370
	CFS	1.0596	1.0748	1.0963	0.9851	0.7638
20	FEM L2x2	1.1186	1.1374	1.1658	1.0411	0.79992
	FEM L4x4	1.0758	1.0936	1.1204	1.0012	0.76982
	FEM Q2x2	1.0623	1.0789	1.1047	0.98717	0.75924
	FEM Q4x4	1.0619	1.0794	1.1057	0.98821	0.76003
	CFS	1.0619	1.0795	1.1058	0.9883	0.7601
10	FEM L2x2	1.1281	1.1565	1.2012	1.0513	0.78946
	FEM L4x4	1.0842	1.1106	1.1522	1.0104	0.76022
	FEM Q2x2	1.0704	1.0953	1.1354	0.99620	0.74996
	FEM Q4x4	1.0700	1.0958	1.1364	0.99718	0.75070
	CFS	1.0701	1.0959	1.1365	0.9973	0.7508
5	FEM L2x2	1.1625	1.2228	1.2972	1.0713	0.77331
	FEM L4x4	1.1150	1.1703	1.2406	1.0293	0.74474
	FEM Q2x2	1.1001	1.1529	1.2213	1.0147	0.73473
	FEM Q4x4	1.0998	1.1534	1.2224	1.0157	0.73545
	CFS	1.0998	1.1535	1.2224	1.01574	0.7355

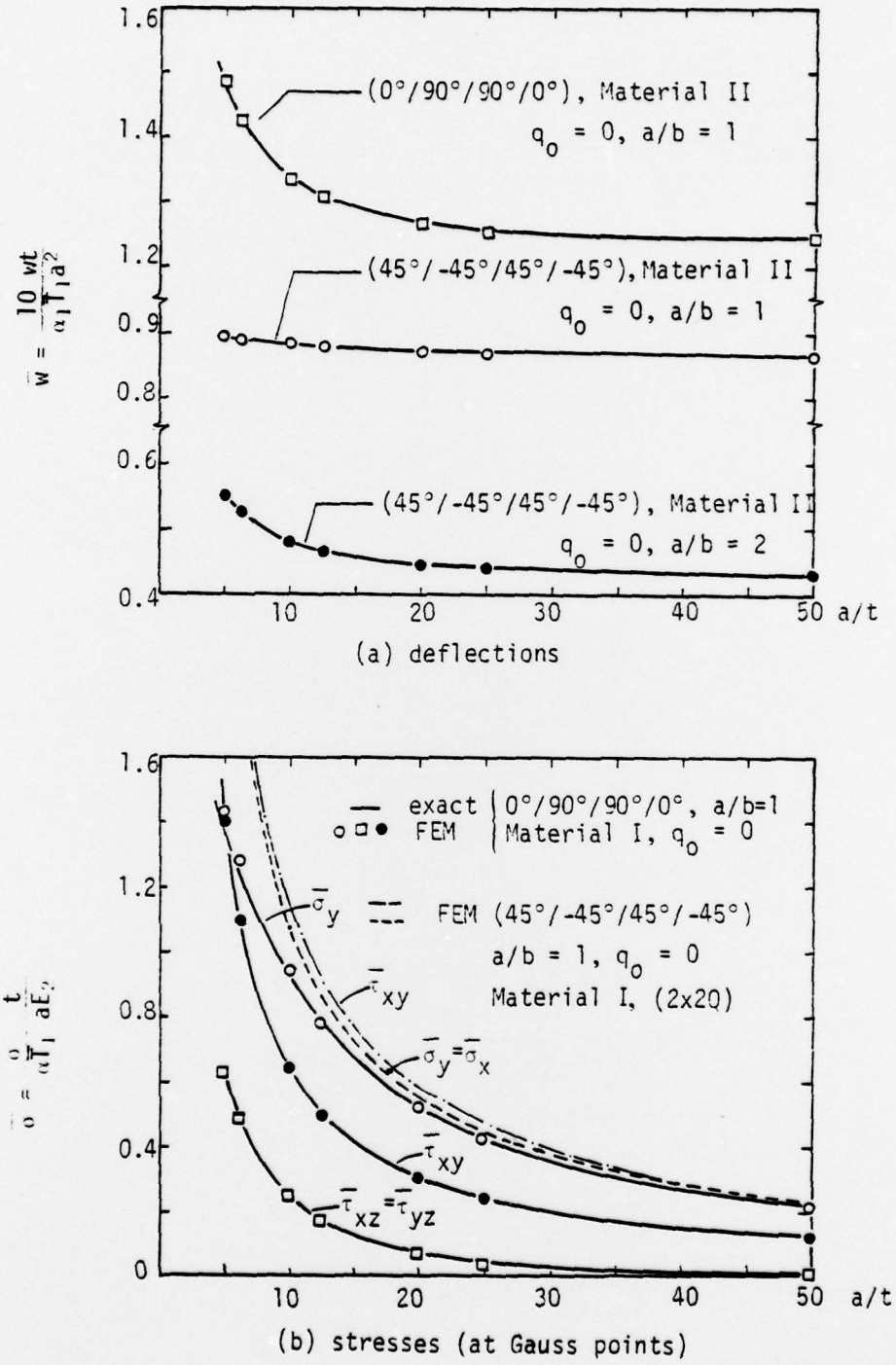

Figure 4 Effect of thickness on the thermal response of cross-ply and angle-ply simply supported plates

Table 9 Effects of side-to-thickness ratio, integration, and type of element on the nondimensionalized fundamental frequency $=(\omega a^2/t)\sqrt{R/E_2}$ of a three-layer cross-ply (0°/90°/0°, $t_1 = t_3 = t/4$, $t_2 = t/2$) square plate (Material II).

a/t	8-Node Element			9-Node Element			closed-form solution
	R	RF	F	R	RF	F	
2	5.503	5.501	5.501	5.504	--	5.502	5.500
4	9.405	9.397	9.396	9.400	9.394	9.402	9.395
5	10.851	10.852	10.858	10.853	10.867	10.858	10.854
6.25	12.341	12.335	12.341	12.346	12.338	12.339	12.331
10	15.178	15.305	15.170	15.208	15.100	15.173	15.145
12.5	16.286	16.278	16.242	16.192	16.291	16.554	16.189
20	17.682	17.579	17.767	17.883	17.409	18.549	17.665
25	18.011	18.149	18.193	18.133	18.049	17.655	18.093
50	18.467	17.518	18.838	18.937	19.644	19.776	18.675
100	22.537	18.701	21.882	19.659	20.507	25.036	18.733

Figure 5a shows the effect of side-to-thickness ratio on the nondimensionalized fundamental frequency of cross-ply rectangular plates (Material II). Similar results are presented for angle-ply plates in Figure 5b. Note again, that the frequencies predicted by the physical symmetry boundary conditions (in FEM) are substantially different from the closed-form solution for two-layer (45°/-45°) angle-ply plates. However, for eight-layer angle-ply plates, this difference vanishes. Figure 5b also shows the nondimensionalized frequency versus the lamination angle for four-layer angle-ply plates (a/b = 1, a/t = 10, Material II). The finite-element solutions with both types of symmetry boundary conditions are close to the closed-form solution and the differences can be seen on the plot.

SUMMARY AND CONCLUSIONS

In this study we investigated the effect of mesh, element type, numerical integration (full and reduced), and boundary conditions on the accuracy of deflections, stresses and natural frequencies associated with cross-ply as well as antisymmetric angle-ply plates by comparing the solutions with the closed-form solutions developed herein. The finite-element solutions are found to be in close agreement with the closed-form solutions for only 2 by 2 mesh of quadratic elements in the quarter plate (for 4 by 4 mesh, they are almost identical to the corresponding closed-form solutions). The closed-form solution for angle-ply plates imply nonphysical symmetry boundary conditions, and its effect on deflections and natural frequencies is discussed. Reduced integration is essential for the analysis of thin plates, but it is not crucial for thick plates.

The element developed herein has been applied to the analysis of bimodulus (materials having different properties in tension and compression)

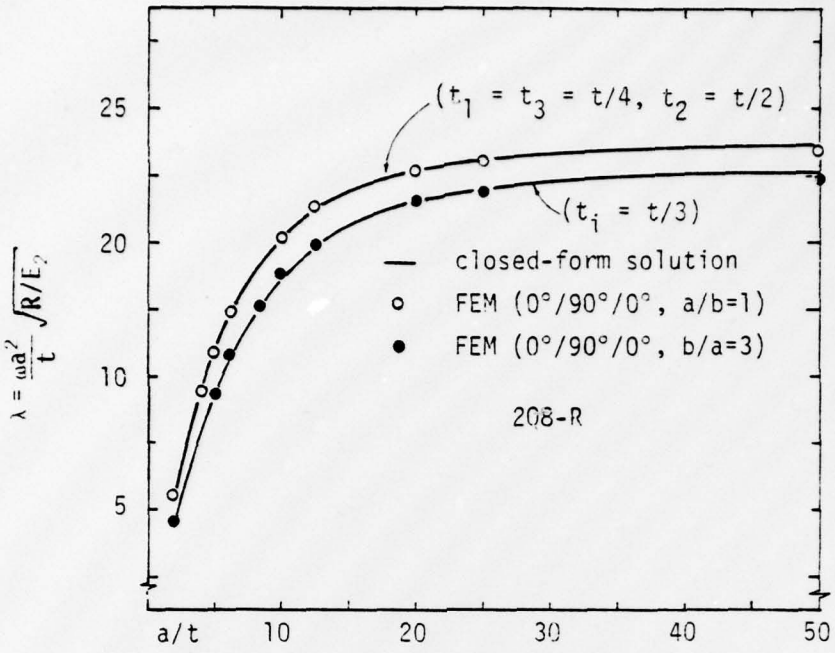

a. Cross-ply plates

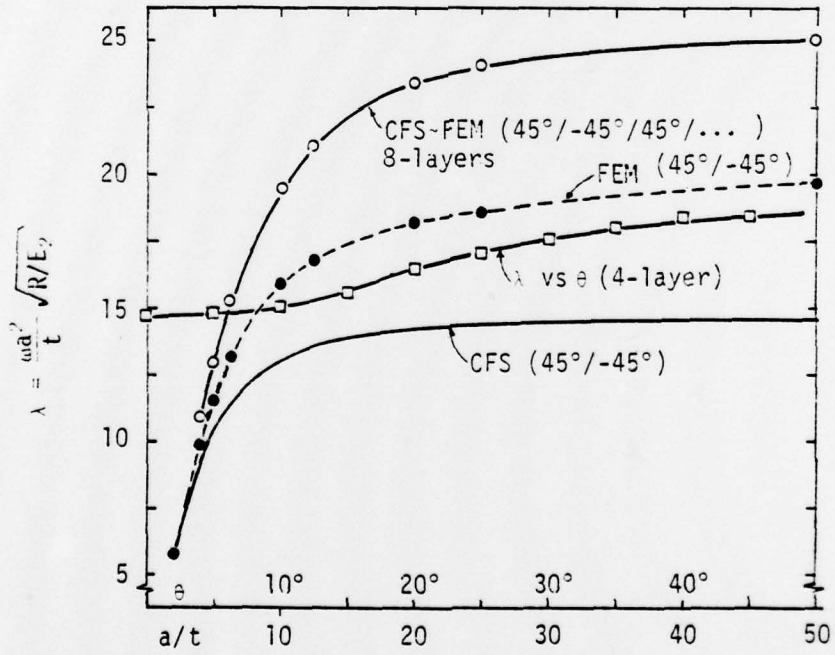

b. Angle-ply plates

Figure 5 Effect of side-to-thickness ratio on the non-dimensionalized natural frequencies of composite plates (Material II)

composite plates by Bert et al. [16], and Reddy and Chao [17]. Application of the present element to transient dynamic analysis is awaiting.

Acknowledgment The results presented herein were obtained during an investigation supported by the Structural Mechanics Program, Office of Naval Research, Arlington, Virginia. Our sincere thanks are also due to Dr. C. W. Bert.

REFERENCES

1. P. C. Yang, C. H. Norris, and Y. Stavsky, Elastic Wave Propagation in Heterogeneous Plates, Int. J. Solids and Structures, Vol. 2, pp. 665-684, 1966.

2. J. M. Whitney and N. J. Pagano, Shear Deformation in Heterogeneous Anisotropic Plates, J. Appl. Mech., Vol. 37, pp. 1031-1036, 1970.

3. J. N. Reddy, Simple Finite Elements with Relaxed Continuity for Nonlinear Analysis of Plates, in Finite Element Methods in Engineering (edited by A. P. Kabaila and V. A. Pulmano), The University of New South Wales, Sydney, Australia, pp. 265-281, 1979.

4. J. N. Reddy, A Penalty Plate-Bending Element for the Analysis of Laminated Anisotropic Composite Plates, Int. J. Numer. Meth. Engng., to appear.

5. C. W. Pryor, Jr. and R. M. Barker, A Finite Element Analysis Including Transverse Shear Effects for Applications to Laminated Plates, AIAA J., Vol. 9, pp. 912-917, 1971.

6. A. S. Mawenya and J. D. Davies, Finite Element Bending Analysis of Multilayer Plates, Int. J. Numer. Meth. Engng., Vol. 8, pp. 215-225, 1974.

7. A. K. Noor and M. D. Mathers, Anisotropy and Shear Deformation in Laminated Composite Plates, AIAA J., Vol. 14, pp. 282-285, 1976.

8. S. C. Panda and R. Natarajan, Finite Element Analysis of Laminated Composite Plates, Int. J. Numer. Meth. Engng., Vol. 14, pp. 69-79, 1979.

9. O. C. Zienkiewicz, R. L. Taylor, and J. M. Too, Reduced Integration Technique in General Analysis of Plates and Shells, Int. J. Numer. Meth. Engng., Vol. 3, pp. 575-586, 1971.

10. T. J. R. Hughes, M. Cohen, and M. Haroun, Reduced and Selective Integration Techniques in the Finite Element Analysis of Plates, Nuclear Engng. & Design, Vol. 46, No. 1, pp. 203-222, 1978.

11. J. M. Whitney, Stress Analysis of Thick Laminated Composite and Sandwich Plates, J. Composite Materials, Vol. 6, pp. 426-440, 1972.

12. N. J. Pagano and S. J. Hatfield, Elastic Behavior of Multilayered Bidirectional Composites, AIAA Journal, Vol. 10, pp. 931-933, 1972.

13. N. J. Pagano, Exact Solutions for Rectangular Bidirectional Composites and Sandwich Plates, J. Composite Materials, Vol. 4, pp. 20-24, 1970.

14. S. W. Tsai, Structural Behavior of Composite Materials, NASA CR-71, July, 1964.

15. C. W. Bert and T. L. C. Chen, Effect of Shear Deformation on Vibration of Antisymmetric Angle-Ply Laminated Rectangular Plates, Int. J. Solids and Structures, Vol. 14, pp. 465-473, 1978.

16. C. W. Bert, J. N. Reddy, V. Sudhakar Reddy, and W. C. Chao, Analysis of Thick Rectangular Plates Laminated of Bimodulus Composite Materials, AIAA/ASME/ASCE/AHS 21st Structures, Structural Dynamics and Materials Conference, Seattle, May 12-14, 1980.

17. J. N. Reddy and W. C. Chao, Finite-Element Analysis of Bimodulus Composite-Material Plates, Computers and Structures, to appear.

PREVIOUS REPORTS ON THIS CONTRACT

Tech. Rept. No.	OU-AMNE Rept. No.	Title of Report	Author(s)
1	79-7	Mathematical Modeling and Micromechanics of Fiber-Reinforced Bimodulus Composite Materials	C.W. Bert
2	79-8	Analyses of Plates Constructed of Fiber-Reinforced Bimodulus Materials	J.N. Reddy and C.W. Bert
3	79-9	Finite-Element Analyses of Laminated-Composite-Material Plates	J.N. Reddy
4A	79-10A	Analyses of Laminated Bimodulus Composite Material Plates	C.W. Bert
5	79-11	Recent Research in Composite and Sandwich Plate Dynamics	C.W. Bert
6	79-14	A Penalty-Plate Bending Element for the Analysis of Laminated Anisotropic Composite Plates	J.N. Reddy
7	79-18	Finite-Element Analysis of Laminated Bimodulus Composite-Material Plates	J.N. Reddy and W.C. Chao